Computer Modeling in Engineering & Sciences

Tech Science Press

Doi:10.32604/cmes.2025.063196

ARTICLE

Numerical Analysis of Entropy Generation in Joule Heated Radiative Viscous Fluid Flow over a Permeable Radially Stretching Disk

Tahir Naseem[1], Fateh Mebarek-Oudina[2,3,*], Hanumesh Vaidya[4], Nagina Bibi[5], Katta Ramesh[6,7] and Sami Ullah Khan[8]

[1]Government Degree College Khanpur, Haripur, 22620, Pakistan
[2]Department of Mathematics, Saveetha School of Engineering, SIMATS, Chennai, 602105, India
[3]Department of Physics, Faculty of Sciences, University of 20 Août 1955-Skikda, B.P 26 Road El-Hadaiek, Skikda, 21000, Algeria
[4]Department of Mathematics, Vijayanagara Sri Krishnadevaraya University, Ballari, 583105, India
[5]Government Girls Degree College No. 2, Haripur, 22620, Pakistan
[6]Department of Pure and Applied Mathematics, School of Mathematical Sciences, Sunway University, Bandar Sunway, Petaling Jaya, 47500, Malaysia
[7]Department of Mathematics, School of Chemical Engineering and Physical Sciences, Lovely Professional University, Jalandhar, 144411, India
[8]Department of Mathematics, Namal University, Mianwali, 42250, Pakistan

*Corresponding Author: Fateh Mebarek-Oudina. Email: f.mebarek_oudina@univ-skikda.dz

Received: 08 January 2025; Accepted: 13 March 2025; Published: 11 April 2025

ABSTRACT: Maximizing the efficiency of thermal engineering equipment involves minimizing entropy generation, which arises from irreversible processes. This study examines thermal transport and entropy generation in viscous flow over a radially stretching disk, incorporating the effects of magnetohydrodynamics (MHD), viscous dissipation, Joule heating, and radiation. Similarity transformations are used to obtain dimensionless nonlinear ordinary differential equations (ODEs) from the governing coupled partial differential equations (PDEs). The converted equations are then solved by using the BVP4C solver in MATLAB. To validate the findings, the results are compared with previously published studies under fixed parameter conditions, demonstrating strong agreement. Various key parameters are analyzed graphically to assess their impact on velocity and temperature distributions. Additionally, Bejan number and entropy generation variations are presented for different physical parameters. The injection parameter ($S < 0$) increases the heat transfer rate, while the suction parameter ($S > 0$) reduces it, exhibiting similar effects on fluid velocity. The magnetic parameter (M) effectively decreases entropy generation within the range of approximately $0 \leq \eta \leq 0.6$. Beyond this interval, its influence diminishes as entropy generation values converge, with similar trends observed for the Bejan number. Furthermore, increased thermal radiation intensity is identified as a critical factor in enhancing entropy generation and the Bejan number.

KEYWORDS: Partial differential equations; modeling; stretched surface; joule heating; viscous dissipation; radiation; suction/injection

1 Introduction

Recent advancements across numerous scientific and technological disciplines have led researchers to explore boundary layer flow over stretched surfaces as an emerging area of study.

When it comes to engineering problems, the flow behaviour of a physical phenomenon toward stretching problems (for both linear and non-linear cases) is critical. The analysis of fluid flow and its entropy

characteristics over a stretching sheet holds significant relevance in various industrial and manufacturing processes. It finds extensive applications in advanced manufacturing techniques such as metal spinning, rubber sheet production, and fiber-reinforced composite manufacturing, including fiberglass fabrication. Additionally, this study is critical in processes like wire drawing, polymer sheet extrusion, and polymer processing, which are integral to the development of high-performance materials. Moreover, the insights gained from such analyses are invaluable in optimizing operations in petroleum industries, where fluid dynamics play a crucial role in processes such as drilling, extraction, and refining. These applications underscore the importance of understanding and controlling fluid behavior for improving efficiency, ensuring product quality, and reducing energy consumption in modern industrial systems. The pace at which the material cools during the technique, as well as the amount of stretching that occurs, determine the desirable qualities of the end product in these conditions. Sakiadis [1–3] analyzed viscous flow over a moving surface using an unsteady incompressible fluid. He investigated the behaviour of boundary layers over continuous surfaces and compared his findings to those of previously published studies [4]. Crane [5] studied continuous viscous flow on a stretched surface in a quiescent fluid with varying velocity. For example, in Hiemenz [6] viscous flow around a stagnation point, the outer flow's free stream velocity is proportional to distance. Crane [7] expanded the work of Sakiadis [3] to include a stretched cylinder and observed that, despite the boundary layer being significantly thicker than the cylinder, the solution remains stable over a long axial distance despite the thicker boundary layer. A comprehensive investigation into magnetohydrodynamic (MHD) mixed convection heat transfer in a lid-driven wavy enclosure with a fin attached to the bottom was conducted by Fayz-Al-Asad et al. [8]. They employed the Galerkin finite element method to solve the governing equations, yielding valuable insights into the complex interactions between fluid flow and thermal dynamics influenced by magnetic fields. Their parametric analysis revealed that the dimensions of the fin, in addition to the Hartmann and Richardson numbers, play a crucial role in determining flow patterns, temperature distribution, and heat transfer effectiveness. Specifically, it was found that longer fins significantly enhance heat transfer under certain conditions, highlighting the potential of these surfaces to optimize fluid mixing, reduce operational costs, and increase thermal efficiency in enclosure systems.

Furthermore, the study leveraged similarity transformations alongside MATLAB's bvp4c solver, which indicated that higher Weissenberg numbers enhance flow velocities while concurrently diminishing the concentration boundary layer. These findings have important implications for cooling technologies and various industrial applications. In a separate but related work, Sohail et al. [9] investigated the effects of bio-convection in tree-dimensional Casson Nanofluid subjected to an induced magnetic stretching field. Their findings highlight the relevance of this phenomenon in various applications. Additionally, another research effort [10] focused on the numerical analysis of how a magnetic dipole influences the behavior of a radiative ferromagnetic liquid flowing over a porous stretched sheet. There were a lot of academics who were inspired by Crane's work and made important contributions by studying the effects of thermal transportation across stretched sheets (see [11–15]).

Rott [16] studied a viscous flow past a moving wall approaching a stagnation point. Danberg et al. [17] recently studied a variation of this problem where the wall is expanded proportionally to Chakrabarti et al. [18] explored an electrically conducting fluid that moved exclusively owing to wall stretching. They observed that temperature increases with the increase of magnetic parameter. The MHD viscoelastic fluid flow across a stretched surface was studied by Andersson [19]. By analytically analyzing the non-linear boundary layer problem, they demonstrate that the influence of viscoelasticity and external magnetic field are the same. Sohail et al. [20] analyzed the effects of magnetic field and viscous dissipation over stretching sheet for the non-Newtonian nanofluid flow. The pace of cooling affects several industrial items' properties.

A magnetic field can also be used to clear molten metals of non-metallic contaminants. Many researchers have addressed the challenge of stretching surfaces using magneto-hydrodynamics [21–24].

Many specialists [25–28] have recently taken an interest in the study of thermal transportation over radiated material through the stretch surface as a result of its extensive use in engineering and industrial activities. These include rubber manufacturing, colloidal suspension and glass sock manufacture, metal spinning and plastic film drawing, paper and textile production, as well as the food processing and geothermal energy sectors. Radiation occurs often in engineering difficulties. Li et al. [29] discussed the usage of radioactive nanofluid flow in light of its applications. Several researchers have recently looked at heat transport issues. Kumam et al. [30] conducted an in-depth study of Casson fluid dynamics within a rotating channel, focusing on magnetohydrodynamic (MHD) radiative flow and the effects of an internal heat source. The research provides a comprehensive analysis of how these combined influences impact the fluid's behavior, including its velocity, temperature distribution, and energy transfer mechanisms. By addressing the interplay of magnetic fields, radiation, and heat generation, the study offers valuable insights into the applications of Casson fluid in engineering and industrial processes, such as in cooling systems, chemical re-actors, and material processing under complex flow conditions.

The method of minimizing entropy generation is utilized in order to optimize thermal engineering devices with the aim of achieving greater energy efficiency. The availability of engineering equipment is diminished as a result of irreversibilities. The idea of entropy generation serves as a measure to evaluate the degree of irreversibility that is inherent in a particular process. It is crucial to emphasize that the second law of thermodynamics exhibits higher dependability compared to the first law of thermo-dynamics, due to the efficacy limitations of the latter in the domain of heat transfer engineering systems. In recent years, there has been a growing focus among researchers on exploring the practical applications and implications of the second law of thermodynamics within thermal engineering systems. This trend highlights the importance of entropy analysis, energy efficiency, and irreversibility minimization as critical tools for optimizing the performance of engineering systems. By studying the second law, scholars aim to identify and quantify sources of energy loss, thereby enabling the design of more efficient systems across various applications, including power generation, refrigeration, air conditioning, and industrial heat exchangers.

The interest also stems from the increasing demand for sustainable and energy-efficient technologies to address global energy challenges. Understanding the second law facilitates the development of advanced methodologies for energy recovery, waste heat utilization, and process optimization, which are vital for reducing carbon footprints. Furthermore, the integration of the second law's principles into modern computational tools has allowed for more precise simulations and real-world applications, reinforcing its role as a cornerstone in the advancement of thermal engineering. Bejan [31] conducted an investigation into the entropy analysis in a process of convective heat transfer. Shit et al. [32] analyzed an entropy generation in an unsteady two-dimensional magnetohydrodynamic (MHD) nanofluid flow over porous exponentially radiated stretching surface. Building on this work, Shit and Mandal [33] investigated entropy generation in an unsteady MHD flow of Casson nanofluid over a vertically radiated stretching plate using Buongiorno's model. Their results revealed that the Casson parameter significantly increases the entropy number, while thermal radiation intensifies the entropy number near the plate. Within this particular context, several pertinent and noteworthy inquiries are expounded upon within the aforementioned articles [34–37].

The literature review highlights a notable gap in research focusing on axisymmetric flow, particularly over radially stretched surfaces. Shahzad et al. [38] addressed this gap by investigating the unsteady axisymmetric flow and heat transfer phenomena under the combined influences of Ohmic heating, viscosity, magnetic fields, and radiation over a stretched surface, with a particular emphasis on irreversibility effects.

The study stands out for its novel approach of employing a similarity transformation to convert the governing equations into nonlinear coupled ordinary differential equations, which were subsequently, solved numerically using the MATLAB BVP4C solver. The analysis meticulously examines the impact of various physical parameters on velocity and temperature profiles, with results presented both graphically and in tabular form for clarity and comprehensiveness.

The findings not only provide fresh insights into the interplay of multiple physical effects on axisymmetric flow but also demonstrate strong agreement with existing literature, thereby validating the robustness and accuracy of the proposed model. This work contributes significantly to the field by advancing the understanding of complex flow and heat transfer phenomena in radially stretched systems, a topic previously underexplored in the literature.

2 Mathematical Form of Physical Phenomena

Think about the time-dependent heat transfer and radially extended viscous fluid flow represented in Fig. 1 as an example. The Reynolds number (Re) was reportedly low. Consequently, the induced magnetic field can be neglected. The fluid begins to flow as the surface stretches (radially) at a velocity $U_w = \frac{ar}{1-ct}$. $T_w = T_\infty + \frac{br}{1-ct}$, where T_∞ is the ambient temperature, and $T_w > T_\infty$; moreover, $a > 0$, $b \geq 0$, and $c \geq 0$ are all constants (with $ct < 1$), and a and c have dimension t^{-1}. T_w is assumed to be the wall temperature. The mathematical representation of the aforementioned physical phenomena of fluid flow and heat transfer is described by the following coupled partial differential equations (PDEs) [38]:

$$\frac{\partial u}{\partial r} + \frac{u}{r} + \frac{\partial w}{\partial z} = 0, \tag{1}$$

$$\frac{\partial u}{\partial t} + u\frac{\partial u}{\partial r} + w\frac{\partial u}{\partial z} = \nu\left(\frac{\partial^2 u}{\partial z^2}\right) - \frac{\sigma}{\rho}\left(B\left(t\right)^2 u\right), \tag{2}$$

$$\frac{\partial T}{\partial t} + u\frac{\partial T}{\partial r} + w\frac{\partial T}{\partial z} = \frac{k}{\rho Cp}\left(\frac{\partial^2 T}{\partial z^2}\right) + \frac{\mu}{\rho Cp}\left(\frac{\partial u}{\partial z}\right)^2 + \frac{\sigma}{\rho Cp}\left(B\left(t\right)^2 u^2\right) - \frac{1}{\sigma\rho Cp}\frac{\partial}{\partial z}q_{rad}, \tag{3}$$

where q_{rad} presents the radiative heat flux and described by Rosseland approximation [39] as:

$$q_{rad} = -\frac{4}{3}\frac{\sigma_s}{k_e}\frac{\partial T^4}{\partial z} = -\frac{4}{3}\frac{\sigma_s}{k_e}T^3\frac{\partial T}{\partial z},$$

here, k_e and σ_s, denote the mean absorption coefficient and the Stefan-Boltzmann constant, respectively. Assuming the temperature variations within the flow are relatively small, the term T^4 can be approximated using a Taylor series expansion around the ambient temperature T_∞ with higher-order terms being neglected for simplification. As a result, the radiative heat flux q_{rad} can be linearized and expressed in the following form:

$$T^4 \cong 4T_\infty^3 T - 3T_\infty.$$

with the corresponding boundary conditions

$$\left\{\begin{array}{c} u = U_w = \frac{ar}{1-ct}, w = W_0, T = T_W = T_\infty + \frac{br}{1-ct}\ at\ z = 0, \\ u \longrightarrow o, T \longrightarrow T_\infty\ as\ z \longrightarrow \infty. \end{array}\right\}, \tag{4}$$

where W_0 stands for surface mass transfer for injection ($W_0 > 0$) and suction ($W_0 < 0$) and kinematic viscosity are defined as:

$$W_0 = -2\left(\frac{\nu U_w}{r}\right)^{\frac{1}{2}} \text{ and } \nu = \frac{\mu}{\rho}.$$

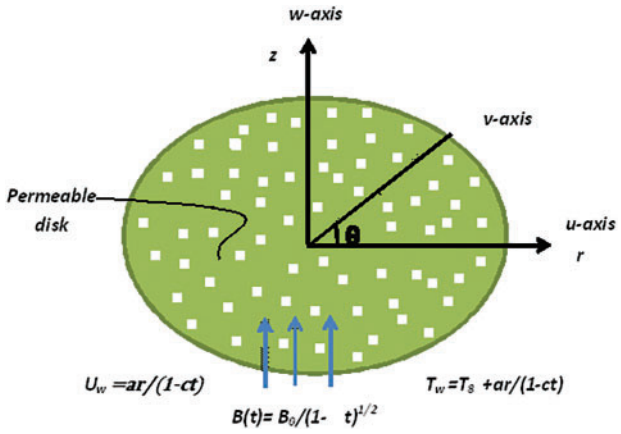

Figure 1: A diagram explains the physics

The dimensionless governing equations are subjected to the similarity transformation given as:

$$\Psi(r,z) = -r^2 U_w Re^{\frac{-1}{2}} f(\eta), \eta = \frac{z}{r} Re^{\frac{1}{2}}, \text{and } \theta(\eta) = \frac{T - T_\infty}{T_w - T_\infty}. \tag{5}$$

The Stokes streams function is defined $u = \frac{-1}{r}\frac{\partial \Psi}{\partial z}$ and $w = \frac{1}{r}\frac{\partial \Psi}{\partial r}$, U_w being the stretching velocity. The velocity component along r and z-axes can be simply computed as follows:

$$u = U_w f'(\eta) \text{ and } w = -2U_w Re^{\frac{-1}{2}} f(\eta), \tag{6}$$

by using the above defined transformation Eqs. (2)–(4) takes the form:

$$f''' + 2ff'' - f'^2 - A\left(f' + \frac{\eta}{2}f''\right) - Mf' = 0 \tag{7}$$

$$\frac{1}{pr}(1+Rd)\theta'' + 2f\theta' - f'\theta + A\left(\theta + \frac{1}{2}\eta\theta'\right) + ME_c f'^2 + \frac{1}{pr}E_c f''^2 = 0 \tag{8}$$

as long as the transform boundary conditions are:

$$f(\eta) = S, f'(\eta) = 1 \text{ and } \theta(\eta) = 1 \; at \; \eta = 0, \tag{9}$$

$$f'(\eta) = 0 \text{ and } \theta(\eta) = 0 \; as \; \eta \longrightarrow \infty, \tag{10}$$

A = a/c is unsteadiness parameter, $Pr = \frac{\mu c_\rho}{k}$ Prandtl number, and mass transfer is denoted by S, where $S > 0$ indicates mass suction and $S > 0$ indicates mass injection. The formulae for the physical quantities Nu and C_f, which are local Nusselt number and skin friction respectively, are given as:

$$C_f = \frac{\tau_w}{\frac{1}{2}\rho U^2} \; and \; N_u = \frac{r q_w}{k\left(T_w - T_\infty\right)}, \tag{11}$$

where τ_w and q_w are, respectively, known as shear stress (wall) and heat flux (wall) which are mathematically described as:

$$\tau_w = \mu \frac{\partial u}{\partial z}\bigg| z = 0 \text{ and } q_w = -k\left(\frac{\partial T}{\partial z}\right)\bigg| z = 0. \tag{12}$$

hence Eq. (11) takes the form:

$$\frac{1}{2} Re^{\frac{1}{2}} C_f = f''(0), Re^{\frac{-1}{2}} N_u = -\theta'(0). \tag{13}$$

2.1 Mathematical Description of Entropy

The volumetric rate of entropy generation in the presence of a magnetic field and radiation number for a viscous fluid is defined as [40,41]:

$$S_g = \underbrace{\frac{k}{{T_\infty}^2}\left(1 + \frac{4}{3}Rd\right)\left(\frac{\partial T}{\partial z}\right)^2}_{} + \underbrace{\frac{\mu}{T_\infty}\left(\frac{\partial u}{\partial z}\right)^2}_{} + \underbrace{\frac{\sigma}{T_\infty} B^2 u^2}_{}, \tag{14}$$

Eq. (14) highlights the various sources of entropy generation. The first term corresponds to the irreversibility caused by heat transfer along a finite temperature gradient, while the remaining two terms account for the contributions of fluid friction and magnetic effect to local entropy generation. By applying the transformation specified in Eq. (5), the non-dimensional form of Eq. (14) is obtained and is mathematically expressed as follows:

$$N_G = \frac{S_g}{S_0} = (1 + Rd)\frac{Re_r}{X}\theta' + \frac{Re_r BrM}{X\Omega} f'^2 + \frac{Re_r Br}{X\Omega} f''^2, \tag{15}$$

where $S_0 = k\left(T_w - T_\infty\right)^2 / T_\infty L^2$ is the entropy (characteristic) rate, $\Omega = \left(T_w - T_\infty\right)/T_w$, the temperature difference (dimensionless), $Re_r = U_w r/v$, the local Reynold's number, $Br = \mu U_w^2 / k\Delta T$, the Brinkman number, and $X = r/L$, the axial distance(dimensionless).

The Bejan number, a crucial variable in the irreversibility distribution, is defined as follows:

$$\text{Be} = \frac{(1 + Rd)\frac{Re_r}{X}\theta'}{\left(1 + \frac{4}{3}Rd\right)\frac{Re_r}{X}\theta' + \frac{Re_r BrM}{X\Omega} f'^2 + \frac{Re_r Br}{X\Omega} f''^2} \tag{16}$$

It can be inferred from Eq. (16) that the Bejan number is constrained within the range of 0 to 1. When the value of Be exceeds 0.5, the dominant factor affecting entropy is the transfer of heat, while when Be is less than 0.5, the primary contributors to entropy are viscous dissipation and the magnetic field. At a magnetic field strength of Be = 0.5, the impact of fluid friction and magnetic field is commensurate with that of entropy resulting from heat transfer.

2.2 Solution Methodology

To deal with the nonlinear complicated issues that arise in mathematical physics, several numerical [17,19,42] and analytical approaches [43] are available. Due to significant nonlinearity, complex geometry, and mixed boundary conditions, it is not possible to obtain precise solutions for all cases. Fig. 2 presents the flow chart for BVP4C.

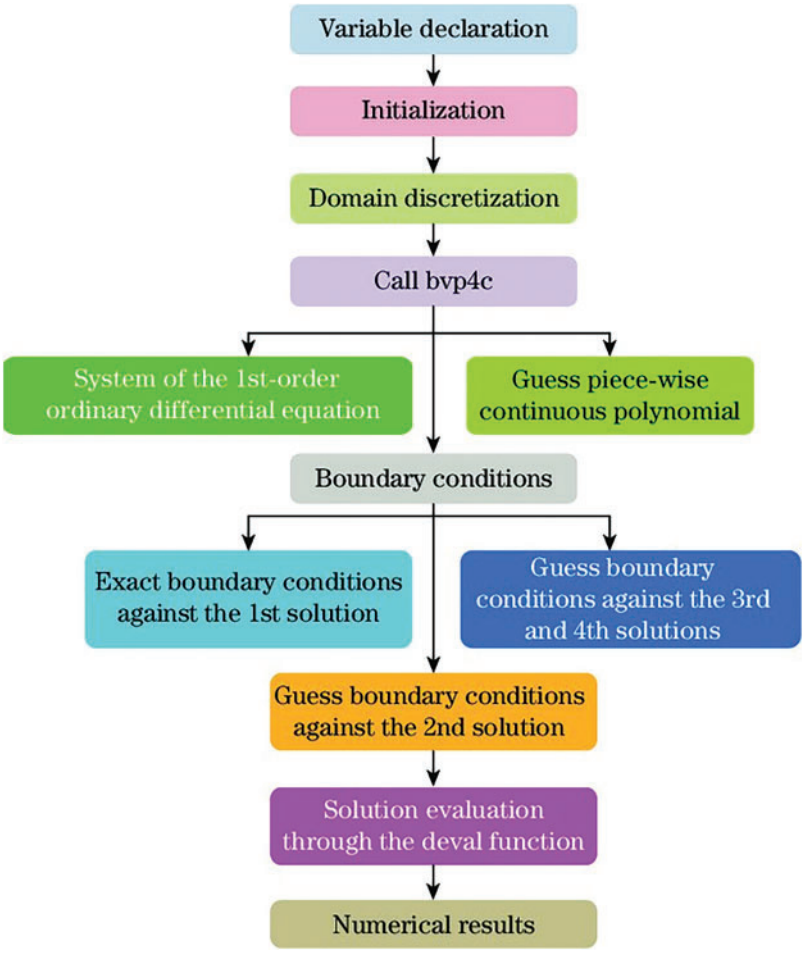

Figure 2: Flow chart of BVP4C

The BVP4C computational method is employed to ascertain the solution of a nonlinear system of ordinary differential equations, specifically Eqs. (7) and (8), while taking into account the boundary conditions outlined in Eqs. (9) and (10). By means of similarity transformation, it is possible to reduce third- and second-order nonlinear ordinary differential equations to first-order difference equations.

$$f = y_1, f' = y_2, f'' = y_3, f''' = -2y_1y_3 + {y_2}^2 + A\left(y_2 + \frac{t}{2}y_3 + My_2\right), \tag{17}$$

$$\theta = y_4, \theta' = y_5, \theta'' = \frac{Pr}{(1+Rd)}\left[-2y_1y_5 + y_2y_4 - A\left(y_4 + \frac{t}{2}y_5\right) - MEc{y_2}^2 - \frac{1}{Pr}{y_3}^2\right], \tag{18}$$

and subject to conditions

$$y_1(0) = S, y_2(0) = 1, y_4(0) = 1, y_2(\infty) = 0, y_4(\infty) = 0. \tag{19}$$

Similarly, the Eqs. (15) and (16) can be expressed as:

$$N_G = \frac{S_g}{S_0} = \left(1 + \frac{4}{3}Rd\right)\frac{Re_r}{X}y_5 + \frac{Re_r BrM}{X\Omega}{y_2}^2 + \frac{Re_r Br}{X\Omega}{y_3}^2, \tag{20}$$

and

$$\mathrm{Be} = \frac{\left(1 + \frac{4}{3}Rd\right)\frac{Re_r}{X}y_5}{\left(1 + \frac{4}{3}Rd\right)\frac{Re_r}{X}y_5 + \frac{Re_r BrM}{X\Omega}{y_2}^2 + \frac{Re_r Br}{X\Omega}{y_3}^2}. \tag{21}$$

with the proper level of precision, the iterative procedure will come to an end.

3 Outcomes and Discussion

The mathematical model in this study is numerically analyzed to evaluate the effects of various factors, including magnetohydrodynamics (MHD), radiation, dissipation, Joule heating, entropy generation number, and Bejan number. The analysis incorporates appropriate boundary conditions. The physical phenomena, involving momentum and energy, are described by nonlinear partial differential equations (PDEs) in both time and space. These PDEs are transformed into a system of nonlinear ordinary differential equations (ODEs) using a suitable similarity transformation. The resulting ODEs are solved numerically using the BVP4C method in MATLAB, ensuring adherence to the relevant boundary conditions. The influence of parameters such as A, (unsteadiness parameter), $S > 0$, (suction parameter), $S < 0$, (injection parameter), and the magnetic parameter on velocity and temperature is analyzed and presented graphically. Additional graphs illustrate the effects of the Prandtl number, Eckert number, and magnetic parameter on the temperature profile. Furthermore, the entropy generation number and Bejan number are graphically depicted. Default parameter values are specified in the descriptions accompanying each figure.

3.1 Impacts of Physical Parameters on Velocity Profile

Fig. 3 depicts the effect of the unsteadiness parameter on velocity profiles. The results reveal that increasing the unsteadiness parameter reduces velocity profiles, which corresponds to a decrease in the momentum thickness of the boundary layer. This reduction indicates that the unsteadiness parameter lowers the flow rate induced by the stretched disk.

Figs. 4 and 5 demonstrate that suction decreases fluid velocity, while injection increases it. Physically, this occurs because a stronger blowing force (injection) pushes the heated fluid farther from the wall, positioning it in a region where buoyant forces enhance flow with a reduced viscosity effect. Consequently, this action increases shear forces and elevates the maximum velocity within the boundary layer. Suction operates in the reverse manner, pulling fluid toward the wall and reducing flow velocity.

Fig. 6 illustrates how changes in the magnetic field influence fluid velocity. As the magnetic parameter (M) increases, the boundary layer thickness and fluid velocity de-crease. This behavior is attributed to the Lorentz force, a resistive body force generated by the magnetic field that impedes fluid motion. Higher magnetic flux amplifies this resistance, further reducing the fluid's velocity.

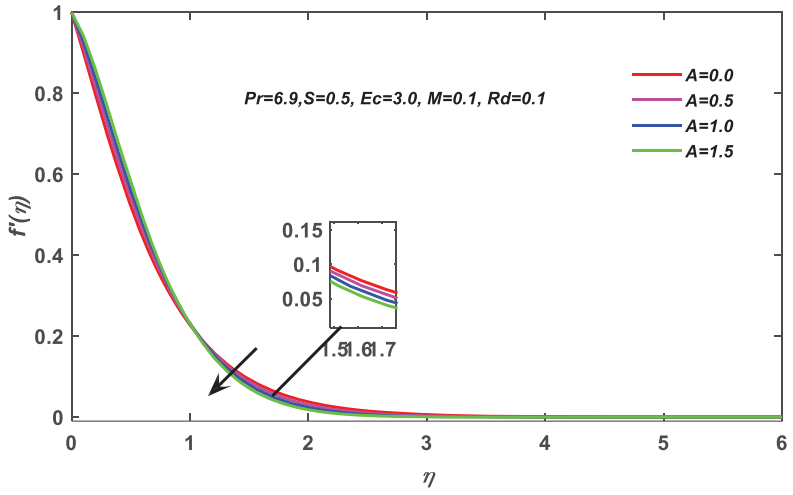

Figure 3: Unsteadiness parameter (A) vs. velocity profile

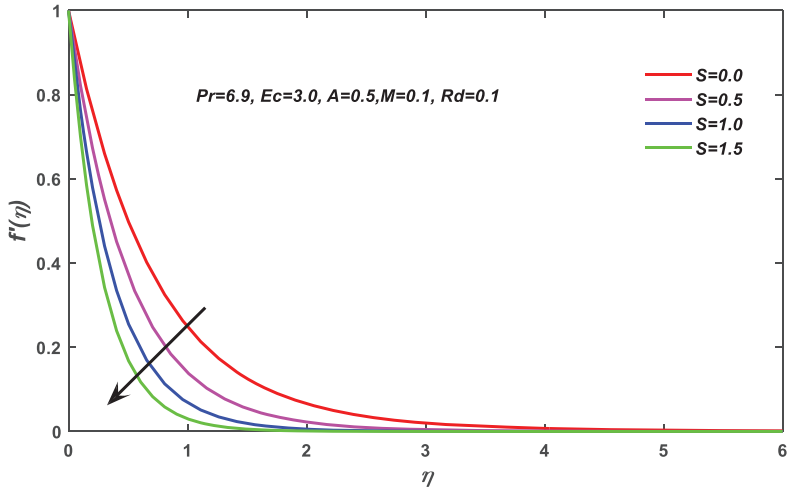

Figure 4: Suction parameter ($S > 0$) vs. velocity profile

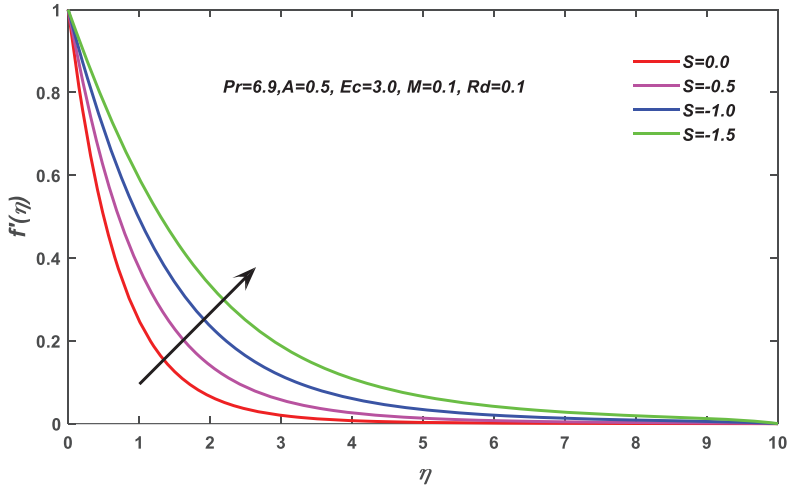

Figure 5: Injection parameter ($S < 0$) vs. velocity profile

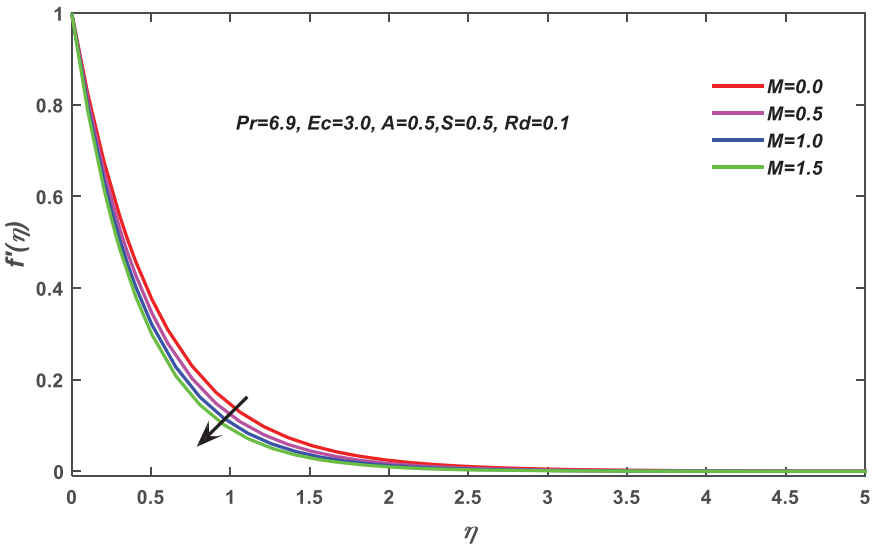

Figure 6: Magnetic parameter (M) vs. velocity profile

3.2 Impacts of Physical Parameters on Temperature Profile

The effect of unsteadiness parameter A on the temperature profile is shown in Fig. 7. The temperature profile exhibits a decreasing trend as the unsteadiness parameter A increases, as depicted in the given figure. The data indicates that the cooling rate is significantly accelerated for larger values of A, whereas the cooling process may exhibit a prolonged duration during a state of constant flow. The Prandtl number Pr is seen in Fig. 8. As the Prandtl number Pr grows, thermal diffusivity decreases, resulting in a decrease in temperature. The effect of suction and injection parameter is presented in Figs. 9 and 10 on the temperature field. From Fig. 9, it is clear that with the increasing parameter of suction the temperature profile decreases while the reverse behaviour is noted for of injection parameter on the temperature profile this is because of reduction of thickness of the thermal boundary layer as a result of suction at ambient temperatures whereas, with injections, the same principle holds true but in the other way.

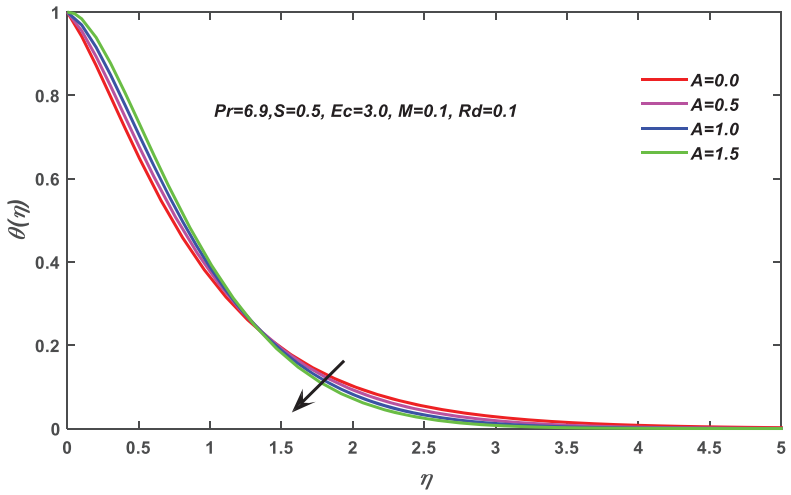

Figure 7: Unsteadiness parameter (A) vs. temperature profile

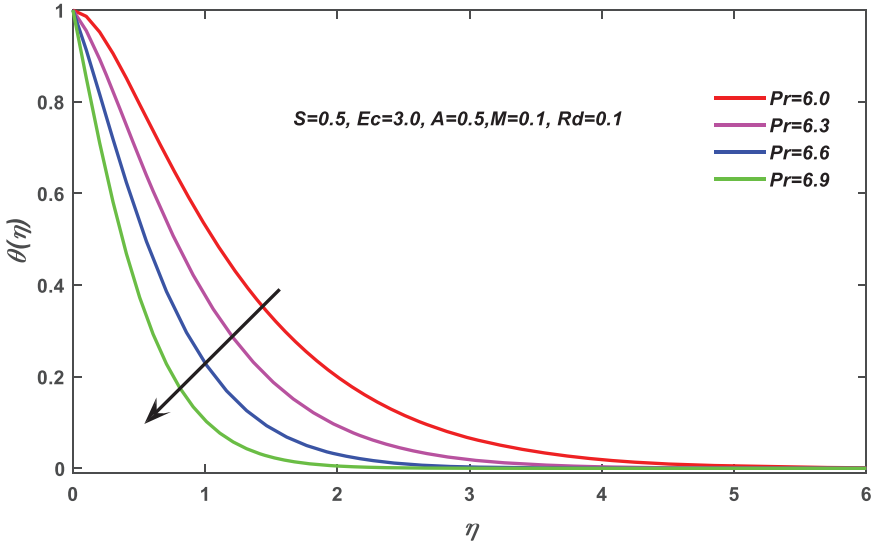

Figure 8: Prandtl number (Pr) vs. temperature profile

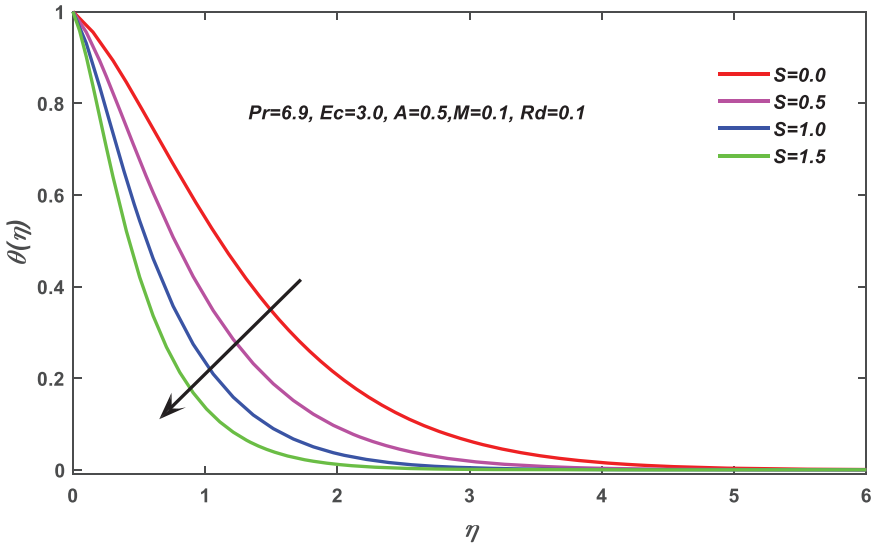

Figure 9: Suction parameter $(S > 0)$ vs. temperature profile

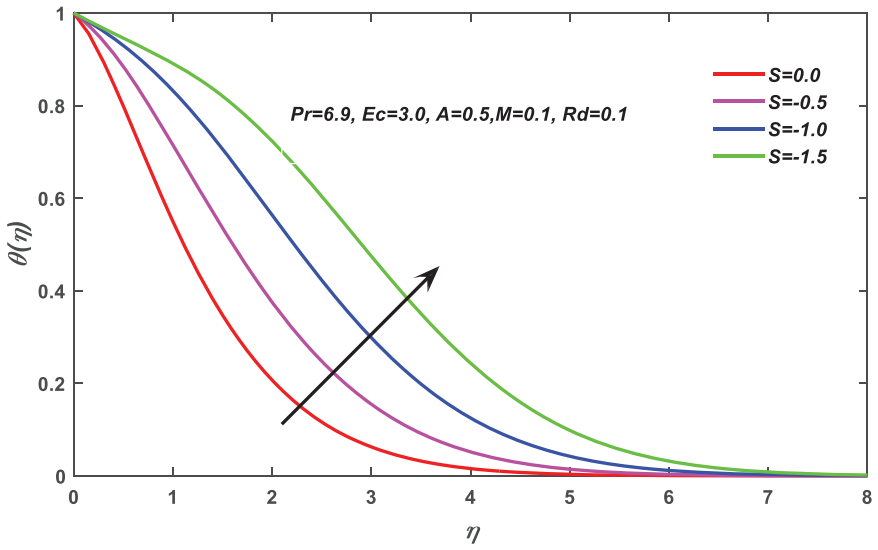

Figure 10: Injection parameter ($S < 0$) vs. temperature distribution

Fig. 11 illustrates the effect of the Eckert number (Ec) on the temperature distribution. A positive correlation is observed, indicating that as Ec increases, the temperature profile also rises. The Eckert number represents the ratio of kinetic energy to enthalpy in the flow. This reflects the conversion of kinetic energy into internal energy due to viscous forces. Higher Ec values signify greater kinetic energy, which leads to intensified molecular vibrations and collisions within the fluid. These increased collisions enhance heat dissipation in the boundary layer, thereby raising the temperature profile in this region.

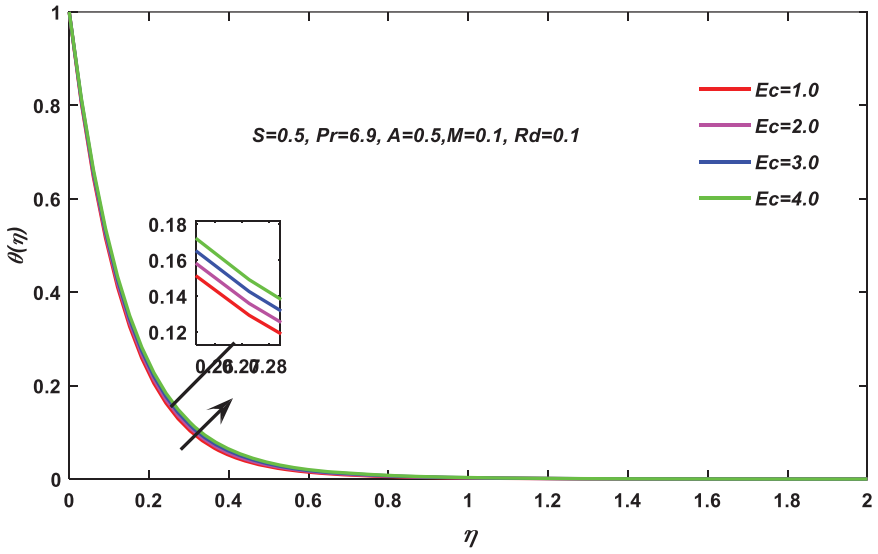

Figure 11: Eckert number (Ec) vs. temperature distribution

Fig. 12 shows the influence of the radiation parameter (Rd) on the temperature profile. As Rd increases, the temperature profile also rises. This is consistent with theoretical expectations since Rd represents the

balance between conduction and radiative heat transfer. A higher Rd indicates a greater contribution of radiative heat transfer, leading to an increase in the temperature profile.

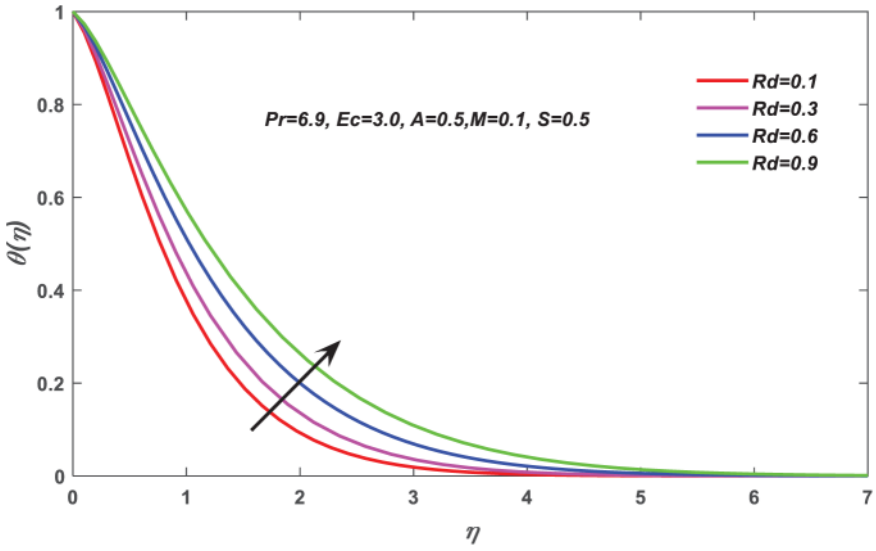

Figure 12: Radiation (Rd) parameter vs. temperature profile

Fig. 13 demonstrates the effect of the magnetic parameter (M) on the temperature profile. As M increases, the velocity profile within the boundary layer decreases due to the Lorentz force, which resists fluid motion. This reduction in velocity leads to higher thermal energy retention in the fluid, causing the temperature profile to rise.

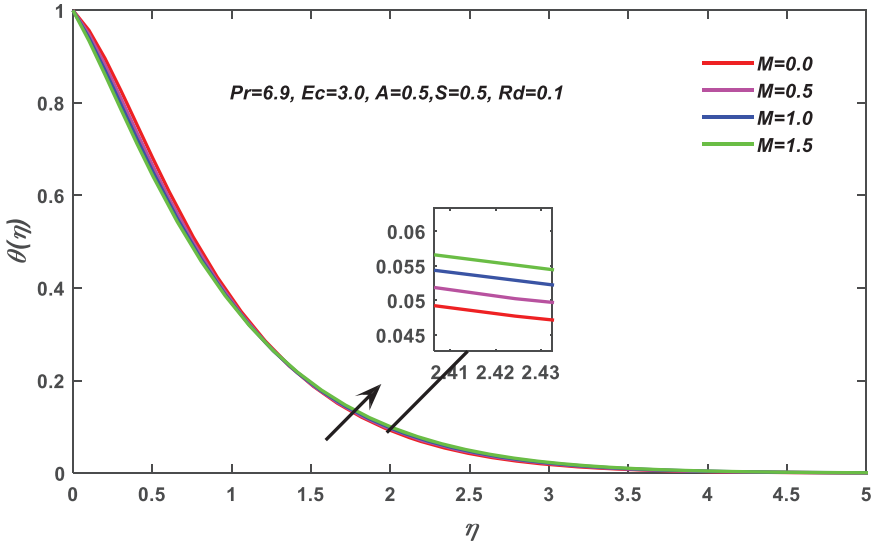

Figure 13: Magnetic parameter (M) vs. temperature profile

Tables 1 and 2 summarize the results of a comparative analysis, showing that the findings of this study align closely with those of previous research conducted by [38], confirming the reliability and accuracy of the present results.

Table 1: Relevant element's effects on surface shear stress

A	S	Pr	$-f''(0)$	
			[38]	Present
0.5	−1	1	0.620400	0.62043436
–	−0.5	–	0.887200	0.88724316
–	0	–	1.308999	1.3086626
–	0.5	–	1.907999	1.9079693
–	1	–	2.655999	2.655588
0	0.5	1	1.798999	1.7986679
0.5	–		1.907999	1.9079693
1	–		2.016999	2.0166622
0.5	0.5	0.5	1.907999	1.9079699
–	–	0.7	1.907999	1.9079694
–	–	1	1.907999	1.9079693

Table 2: Relevant element's effects on local heat transmission

A	S	Pr	$-\theta(0)$	
			[38]	Present
0.5	−1	1	0.620400	0.10992243
–	−0.5	–	0.887200	0.21888713
–	0	–	1.308999	0.45448468
–	0.5	–	1.907999	0.79851912
–	1	–	2.655999	1.2097214
0	0.5	1	1.798999	0.98038262
0.5	–		1.907999	0.79851912
1	–		2.016999	0.60799946
0.5	0.5	0.5	1.119999	0.011034301
–	–	0.7	1.450000	0.33052076
–	–	1	1.907999	0.79851912

3.3 Impacts of Physical Parameters on Entropy Generation and Bejan Numbers

Figs. 14 and 15 illustrate the effect of the magnetic parameter (M) on entropy generation (N_G) and the Bejan number (Be). As shown in Fig. 14, an initial increase in M reduces entropy generation near the disk. However, at higher values of M, entropy generation begins to increase. A similar trend is observed in Fig. 15 for the Bejan number. This behavior is attributed to the resistive Lorentz force produced at high M, which slows fluid motion. Additionally, a strong magnetic field induces Ohmic heating, leading to a temperature rise and an associated increase in heat generation, thereby contributing to greater entropy production. Away from the disk, for large values of M, heat transfer irreversibility dominates over fluid friction irreversibility.

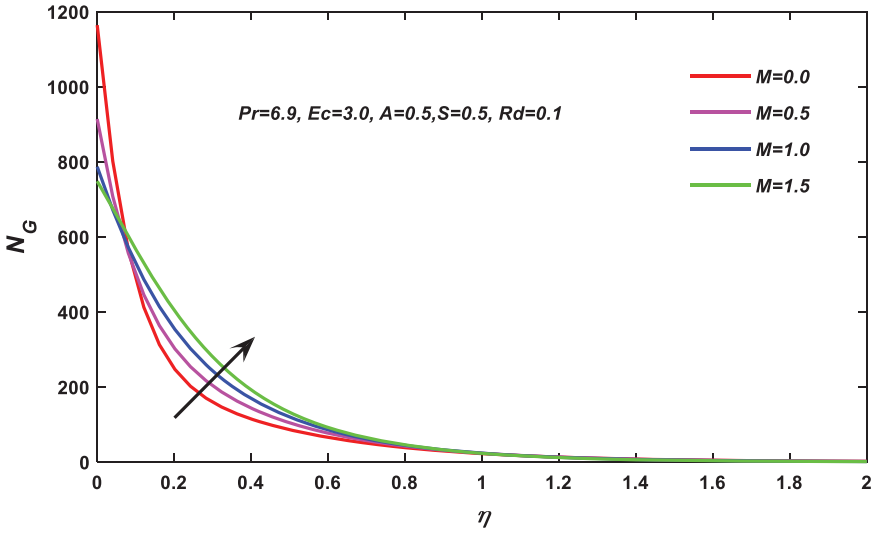

Figure 14: Magnetic parameter (M) vs. entropy generation number

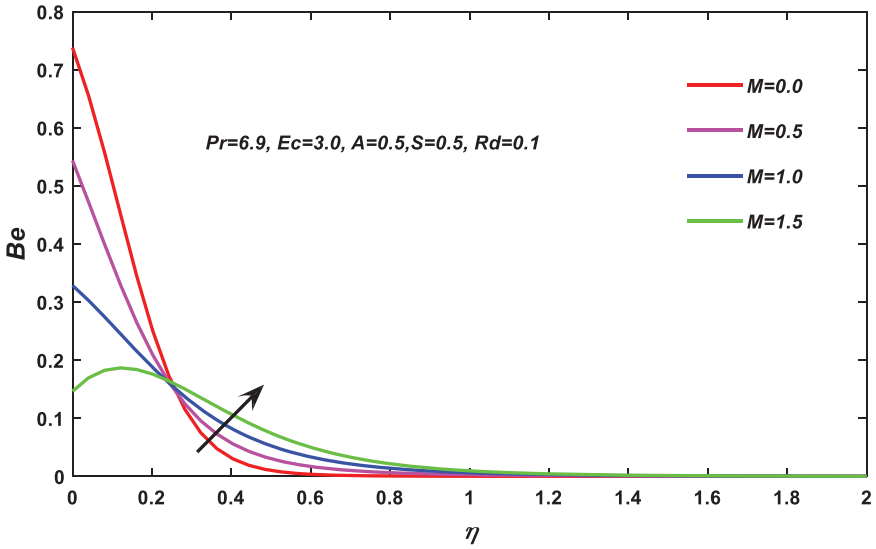

Figure 15: Magnetic parameter (M) vs. Bejan number

Fig. 16 presents the relationship between entropy generation and various values of the Brinkman number (Br). The Brinkman number represents the ratio of heat generated by viscous dissipation to heat transferred through molecular conduction. As Br increases, the conduction rate of heat generated by viscous dissipation decreases, leading to a rise in entropy generation. Fig. 17 shows the variation of the Bejan number with respect to Br, revealing a negative correlation. An increase in Br elevates the overall entropy generation rate, which, in turn, reduces the Bejan number due to the dominant effect of viscous dissipation.

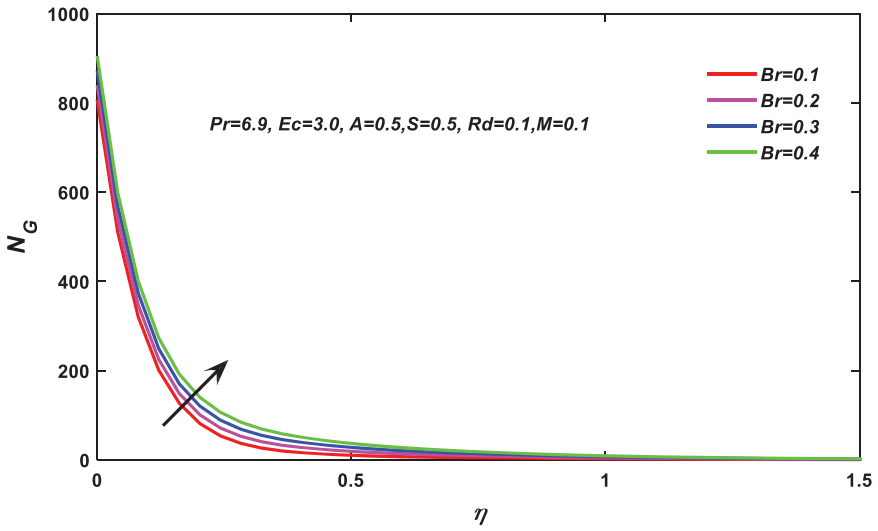

Figure 16: Brickman number (Br) vs. entropy generation number

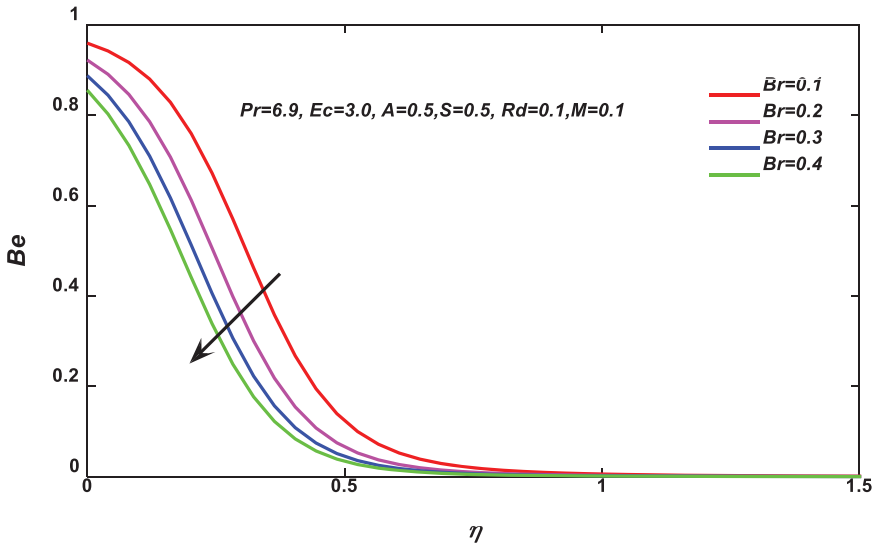

Figure 17: Brickman number (Br) vs. Bejan number

Figs. 18 and 19 demonstrate that an increase in the thermal radiation parameter (Rd) significantly enhances both entropy generation and the Bejan number. Higher temperatures associated with increased Rd amplify radiative heat transfer, leading to greater entropy generation and an elevated Bejan number. In this case, thermal irreversibility becomes the predominant factor contributing to the overall entropy generation.

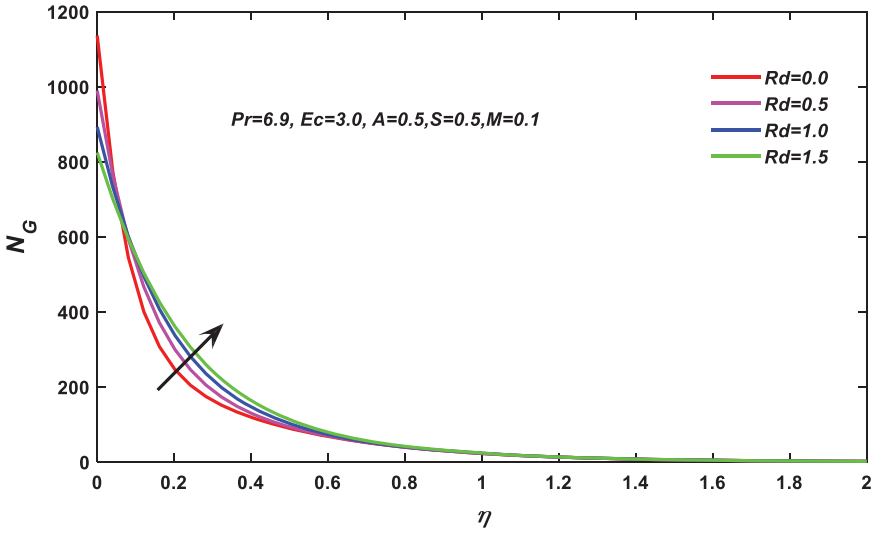

Figure 18: Radiation parameter (Rd) vs. entropy number

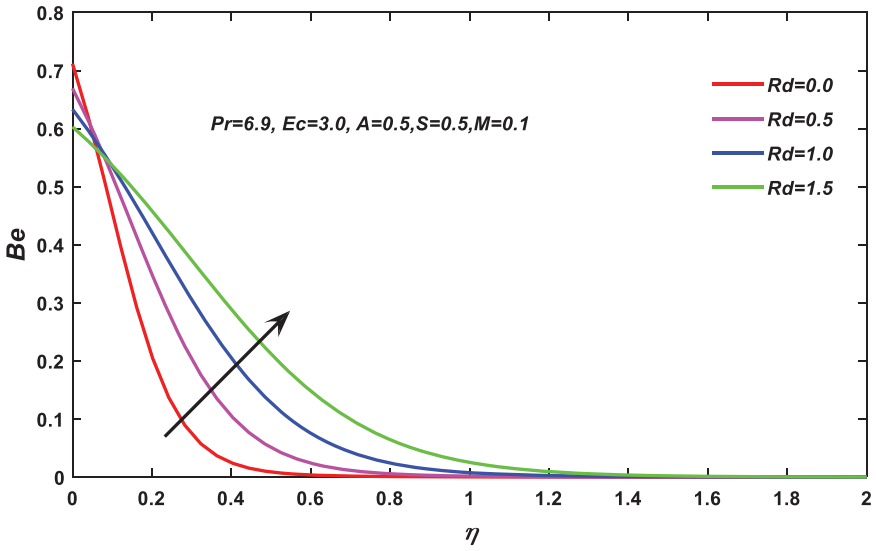

Figure 19: Radiation parameter (Rd) vs. Bejan number

4 Conclusions

This study analyzed entropy generation and thermophysical properties in radiative materials using a radially stretching disk as the model. Tables 1 and 2 detail the effects of various physical parameters on skin friction and the local Nusselt number (wall heat flux and transfer rate). A comparison with previous studies revealed excellent agreement, affirming the validity of the results. The influence of thermophysical properties on flow behavior, entropy generation, and the Bejan number was illustrated and interpreted graphically. The key findings of the analysis are summarized below:

– Increasing the radiation parameter raises the temperature, with a similar trend observed for the magnetic parameter.

- Suction reduces fluid velocity and temperature profiles, while injection increases them.
- The temperature profile decreases with higher Prandtl (Pr) and Eckert (Ec) numbers.
- The magnetic parameter decreases entropy generation near the disk but significantly increases it farther from the disk, a pattern also reflected in the Bejan number.
- Enhanced thermal radiation intensity is a major factor in the elevated production of both entropy and the Bejan number.

Additionally, the utilization of entropy generation analysis in unsteady processes is a more intricate task, as it requires identifying an optimal time history to minimize the entropy generated within a finite time span. For this reason, entropy generation is infrequently applied in addressing transient operations and off-design conditions. These results provide valuable insights into the thermal management of radiative systems and the optimization of energy processes in various engineering applications.

This study is constrained by its focus on a simplified model, which may not fully represent the complexities found in practical applications. Additionally, the investigation did not account for the effects of varying material properties or complex geometries, which could significantly impact the results.

Acknowledgement: The authors acknowledge their affiliations.

Funding Statement: The authors received no specific funding for this study.

Author Contributions: Conceptualization, methodology, software, validation, formal analysis, investigation, resources, data curation, writing—original draft preparation, writing—review and editing, visualization, project administration, funding acquisition: Tahir Naseem, Fateh Mebarek-Oudina, Hanumesh Vaidya, Nagina Bibi, Katta Ramesh, Sami Ullah Khan; supervision, Fateh Mebarek-Oudina. All authors reviewed the results and approved the final version of the manuscript.

Availability of Data and Materials: Not applicable.

Ethics Approval: Not applicable.

Conflicts of Interest: The authors declare no conflicts of interest. The authors assert that they do not possess any associations or engagements with any institution or entity that has any monetary stakes in the topic or materials deliberated in this manuscript.

Nomenclature

a, b, c	Constants
B	Uniform magnetic field (external)
B_0	Magnetic flux density (constant)
k	Thermal conductivity
M	Magnetic parameter
C_p	Specific heat at constant pressure
C_f	Skin friction coefficient
Nu_x	Local Nusselt number
q_w	Surface heat flux
q_w	Surface heat flux
f	Self-similar velocity
u, w	Velocity components
t	Time
T	Temperature
S_g'''	Actual entropy generation rate

S_0'''	Characteristic entropy generation rate
$S > 0$	Suction parameter
$S < 0$	Injection parameter
X	Dimensionless axial distance

Dimensionless Parameters

Ec	Eckert number
Re	Reynolds number
Pr	Prandtl number
A	Unsteadiness parameter
Br	Brinkman number
M	Hartman number
N_G	Entropy generation number
Rd	Radiation parameter

Greek Symbols

η	Similarity variable
ρ	Density
μ	Dynamic viscosity
σ	Electrical conductivity

Subscripts

s	Solid phase
w	Condition of wall
∞	Condition of free stream

References

1. Sakiadis BC. Boundary-layer behavior on continuous solid surfaces: I. Boundary-layer equations for two-dimensional and axisymmetric flow. AIChE J. 1961;7(1):26–8. doi:10.1002/aic.690070108.
2. Sakiadis BC. Boundary-layer behavior on continuous solid surfaces: II. The boundary layer on a continuous flat surface. AIChE J. 1961;7(2):221–5. doi:10.1002/aic.690070211.
3. Sakiadis BC. Boundary-layer behavior on continuous solid surfaces: III. The boundary layer on a continuous cylindrical surface. AIChE J. 1961;7(3):467–72. doi:10.1002/aic.690070325.
4. Blasius H. Grenzschichten in Flüssigkeiten mit kleiner Reibung. Berlin, Germany: Druck von BG Teubner; 1907.
5. Crane LJ. Flow past a stretching plate. Z Für Angew Math Und Phys ZAMP. 1970;21(4):645–7. doi:10.1007/BF01587695.
6. Hiemenz K. Die Grenzschicht an einem in den gleichformigen Flussigkeitsstrom eingetauchten geraden Kreiszylinder. Dinglers Polytech J. 1911;326:321–4.
7. Crane LJ. Boundary layer flow due to a stretching cylinder. Z Für Angew Math Und Phys ZAMP. 1975;26(5):619–22. doi:10.1007/BF01594034.
8. Fayz-Al-Asad M, Mebarek-Oudina F, Vaidya H, Hasan MS, Sarker MMA, Ismail AI. Finite element analysis for magneto-convection heat transfer performance in vertical wavy surface enclosure: fin size impact. Front Heat Mass Transf. 2024;22(3):817–37. doi:10.32604/fhmt.2024.050814.
9. Sohail M, Hussain Shah SQ, Sultan F, Jahan S, Abbas ST. Three-dimensional stretched boundary layer flow of casson nanofluid in rotating frame with bio-convection phenomenon. Sci Iran. 2024. doi:10.24200/sci.2024.63534.8450.
10. Dharmaiah G, Mebarek-Oudina F, Balamurugan KS, Vedavathi N. Numerical analysis of the magnetic dipole effect on a radiative ferromagnetic liquid flowing over a porous stretched sheet. Fluid Dyn Mater Process. 2024;20(2):293–310. doi:10.32604/fdmp.2023.030325.

11. Mallikarjuna HB, Nirmala T, Punith Gowda RJ, Manghat R, Varun Kumar RS. Two-dimensional Darcy-Forchheimer flow of a dusty hybrid nanofluid over a stretching sheet with viscous dissipation. Heat Transf. 2021;50(4):3934–47. doi:10.1002/htj.22058.
12. Sohail M, Ali MH, Abodayeh K, Abbas ST. Bio-convective boundary layer flow of Maxwell nanofluid via optimal homotopic procedure with radiation and Darcy-Forchheimer impacts over a stretched sheet. Int J Ambient Energy. 2025;46(1):2462583. doi:10.1080/01430750.2025.2462583.
13. Sarkar GM, Sahoo B. On dual solutions of the unsteady MHD flow on a stretchable rotating disk with heat transfer and a linear temporal stability analysis. Eur J Mech-B/Fluids. 2021;85:149–57. doi:10.1016/j.euromechflu.2020.09.010.
14. Ramesh K, Mebarek-Oudina F, Souayeh B, editors. Mathematical modelling of fluid dynamics and nanofluids. Boca Raton, FL, USA: CRC Press; 2024.
15. Kumar MA, Mebarek-Oudina F, Mangathai P, Shah NA, Vijayabhaskar C, Venkatesh N, et al. The impact of Soret Dufour and radiation on the laminar flow of a rotating liquid past a porous plate via chemical reaction. Mod Phys Lett B. 2025;39(10):2450458. doi:10.1142/S021798492450458X.
16. Rott N. Unsteady viscous flow in the vicinity of a stagnation point. Q Appl Math. 1956;13(4):444–51. doi:10.1090/qam/74194.
17. Danberg JE, Fansler KS. A nonsimilar moving-wall boundary-layer problem. Q Appl Math. 1976;34(3):305–9. doi:10.1090/qam/99653.
18. Chakrabarti A, Gupta AS. Hydromagnetic flow and heat transfer over a stretching sheet. Q Appl Math. 1979;37(1):73–8. doi:10.1090/qam/99636.
19. Andersson HI. MHD flow of a viscoelastic fluid past a stretching surface. Acta Mech. 1992;95(1):227–30. doi:10.1007/BF01170814.
20. Sohail M, Rafique E, Singh A, Tulu A. Engagement of modified heat and mass fluxes on thermally radiated boundary layer flow past over a stretched sheet via OHAM analysis. Discov Appl Sci. 2024;6(5):240. doi:10.1007/s42452-024-05833-1.
21. Fatunmbi EO, Adeosun AT, Salawu SO. Irreversibility analysis for eyring-powell nanoliquid flow past magnetized riga device with nonlinear thermal radiation. Fluids. 2021;6(11):416. doi:10.3390/fluids6110416.
22. Pattanavanitkul P, Pakdee W. Parametric study of unsteady flow and heat transfer of compressible helium-xenon binary gas through a porous channel subjected to a magnetic field. Fluids. 2021;6(11):392. doi:10.3390/fluids6110392.
23. Abbas N, Shatanawi W, Mustafa Z. Thermal analysis of non-Newtonian fluid with radiation and MHD effects over permeable exponential stretching sheet. Case Stud Therm Eng. 2025;68(1):105895. doi:10.1016/j.csite.2025.105895.
24. Hou E, Wang F, El-Zahar ER, Nazir U, Sohail M. Computational assessment of thermal and solute mechanisms in carreau-yasuda hybrid nanoparticles involving soret and dufour effects over porous surfa. Micromachines. 2024;12(11):1302. doi:10.3390/mi12111302.
25. Shah Z, Islam S, Ayaz H, Khan S. Radiative heat and mass transfer analysis of micropolar nanofluid flow of Casson fluid between two rotating parallel plates with effects of Hall current. J Heat Transf. 2019;141(2):022401. doi:10.1115/1.4040415.
26. Khan AS, Nie Y, Shah Z, Dawar A, Khan W, Islam S. Three-dimensional nanofluid flow with heat and mass transfer analysis over a linear stretching surface with convective boundary conditions. Appl Sci. 2018;8(11):2244. doi:10.3390/app8112244.
27. Mebarek-Oudina F, Dharmaiah G, Rama Prasad JL, Vaidya H, Kumari MA. Thermal and flow dynamics of magnetohydrodynamic burgers' fluid induced by a stretching cylinder with internal heat generation and absorption. Int J Thermophys. 2025;25(3):100986. doi:10.1016/j.ijft.2024.100986.
28. Imran N, Javed M, Qayyum M, Sohail M, Kashif M. Heat transfer analysis for particle-fluid suspension thermomagnetohydrodynamic peristaltic flow with Darcy-Forchheimer medium. Heat Transfer. 2021;50(4):3547–63. doi:10.1002/htj.22040.
29. Li Z, Sheikholeslami M, Shah Z, Shafee A, Al-Qawasmi A, Tlili I. Time dependent heat transfer in a finned triplex tube during phase changing of nanoparticle enhanced PCM. Eur Phys J Plus. 2019;134(4):173. doi:10.1140/epjp/i2019-12627-9.

30. Kumam P, Shah Z, Dawar A, Rasheed HU, Islam S. Entropy generation in MHD radiative flow of CNTs Casson nanofluid in rotating channels with heat source/sink. Math Probl Eng. 2019;2019(1):9158093. doi:10.1155/2019/9158093.
31. Bejan A. Second law analysis in heat transfer. Energy. 1980;5(8–9):720–32. doi:10.1016/0360-5442(80)90091-2.
32. Shit G.C.Haldar R, Mandal S. Entropy generation on MHD flow and convective heat transfer in a porous medium of exponentially stretching surface saturated by nanofluids. Adv Powder Technol. 2017;28(6):1519–30. doi:10.1016/j.apt.2017.03.023.
33. Shit GC, Mandal S. Entropy analysis on unsteady MHD flow of Casson nanofluid over a stretching vertical plate with thermal radiation effect. Int J Appl Comput Math. 2020;6(1):2. doi:10.1007/s40819-019-0754-4.
34. Bartwal P, Upreti H, Pandey AK. Heat transfer assessment of magnetized tangent hyperbolic fluid flow through porous disk using LWCM: application in solar thermal power plant. Nano. 2024;2450157. doi:10.1142/S1793292024501571.
35. Upreti H, Uddin Z, Pandey AK, Joshi N. Particle swarm optimization based numerical study for pressure, flow, and heat transfer over a rotating disk with temperature dependent nanofluid properties. Numer Heat Transf Part A Appl. 2023;83(8):815–44. doi:10.1080/10407782.2022.2156412.
36. Raza J, Mebarek-Oudina F, Ali H, Sarris IE. Slip effects on Casson Nanofluid over a Stretching sheet with activation energy: RSM Analysis. Front Heat Mass Transf. 2024;22(4):1017–41. doi:10.32604/fhmt.2024.052749.
37. Das S, Chakraborty S, Jana RN, Makinde OD. Entropy analysis of unsteady magneto-nanofluid flow past accelerating stretching sheet with convective boundary condition. Appl Math Mech. 2015;36(12):1593–610. doi:10.1007/s10483-015-2003-6.
38. Shahzad A, Ali R, Hussain M, Kamran M. Unsteady axisymmetric flow and heat transfer over time-dependent radially stretching sheet. Alex Eng J. 2017;56(1):35–41. doi:10.1016/j.aej.2016.08.030.
39. Brewster MQ. Thermal radiative transfer and properties. Hoboken, NJ, USA: John Wiley & Sons; 1992.
40. Bejan A. Entropy generation minimization: the method of thermodynamic optimization of finite-size systems and finite-time processes. Boca Raton, FL, USA: CRC Press; 2013.
41. Sajid M, Hayat T, Asghar S. On the analytic solution of the steady flow of a fourth grade fluid. Phys Lett A. 2006;355(1):18–26. doi:10.1016/j.physleta.2006.01.092.
42. Sohail M, Ilyas K, Rafique E, Singh A, Jahan S. OHAM analysis on bio-convective flow of partial differential equations of Casson nanofluid under thermal radiation impact past over a stretching sheet. BioNanoScience. 2024;14(2):1572–82. doi:10.1007/s12668-024-01329-9.
43. Ghasemi SE, Vatani M, Hatami M, Ganji DD. Analytical and numerical investigation of nanoparticle effect on peristaltic fluid flow in drug delivery systems. J Mol Liq. 2016;215(11):88–97. doi:10.1016/j.molliq.2015.12.001.